The Cryosphere Discuss., doi:10.5194/tc-2016-93, 2016
Manuscript under review for journal The Cryosphere
Published: 13 May 2016

The Cryosphere Discussions
Open Access
EGU

Surface-layer turbulence, energy-balance and links to atmospheric circulations over a mountain glacier in the French Alps.

Maxime Litt[1], Jean-Emmanuel Sicart[1,2,3], Delphine Six[4,5], Patrick Wagnon[1,2,3,6], and Warren D. Helgason[7]

[1]Univ. Grenoble Alpes, LTHE, F-38000 Grenoble, France
[2]CNRS, LTHE, F-38000 Grenoble, France
[3]IRD, LTHE, F-38000 Grenoble, France
[4]Univ. Grenoble Alpes, LGGE, F-38000 Grenoble, France
[5]CNRS, LGGE, F-38000 Grenoble, France
[6]Icimod, GPO Box 3226, Kathmandu, Nepal
[7]Civil and Geological Engineering, University of Saskatchewan, 57 Campus Drive, Saskatoon S7N 5A9, Saskatchewan, Canada

Correspondence to: M.Litt (maximelitt@gmail.com)

Abstract. Over mountain glaciers, large errors may affect turbulent surface heat fluxes estimated with the bulk-aerodynamic (BA) method. That might lead to uncertainties in estimating melt from surface energy balance (SEB). During the summers of 2006 and 2009, in the atmospheric surface layer of Saint-Sorlin Glacier (French Alps, 45° N, 6.1° E, $\sim$ 3 km^2), mean air-temperature and wind-speed vertical profiles and high frequency Eddy-Covariance (EC) data were collected to characterize the turbulence and the turbulent fluxes. We studied the influence of the BA method errors on the melt estimations, calculating the SEB alternatively with turbulent fluxes obtained from the BA and the EC methods. We classified our results in terms of large-scale forcing. In weak synoptic forcing, local thermal effects dominated the wind circulation. On the glacier, weak katabatic flows with a wind-speed maximum at low height (2-3 m) were detected 71% of the time and were generally associated with weak turbulent kinetic energy (TKE) and turbulent fluxes. When the large-scale forcing was strong, the wind in the valley aligned with the glacier flow, intense downslope flows were observed, no wind-speed maximum was visible below 5 m, TKE and turbulent fluxes were often intense. For both regimes, the surface layer turbulence production was probably not at equilibrium with dissipation because of the interaction of large-scale orographic disturbances with the flow when the forcing was strong, or low-frequency oscillations of the katabatic flow when the forcing was weak. When TKE was low, all turbulent fluxes calculation methods provided similar fluxes. When TKE was large, the EC method provided larger fluxes than the BA method. This underestimation was compensated by increasing the BA flux estimates using melt-calibrated effective roughness lengths. Though strong forcing was more frequently associated with large TKE events than weak forcing conditions, differences between the different SEB estimates remained in both cases within the error range of observed melt.

The Cryosphere Discuss., doi:10.5194/tc-2016-93, 2016
Manuscript under review for journal The Cryosphere
Published: 13 May 2016

1 Introduction

Climate change might affect the hydrological regimes in englacial mountainous catchments (Viviroli et al., 2011). There is a strong need to understand the links between large-scale atmospheric changes and glacier melt processes. The melt response of glaciers to climate change is generally assessed using calibrated temperature-index models of various complexities (Hock, 2003; Huss et al., 2010; Pellicciotti et al., 2012). Though these models perform correctly when meteorological conditions do not differ much with regard to the calibration period conditions, under changing climate, the frequency of occurrence of specific atmospheric circulation patterns may change (Corti et al., 1999), affecting relationships between temperature and melt. The physical link between glacier melt and climate is the surface energy balance (SEB), embodying all the heat exchanges occurring near the glacier surface (Oke, 1987). Surface energy balance studies under contrasted climatic conditions are required to validate temperature-index calibrations, and adapt them to changing melt processes in a changing climate.

Turbulent energy transfer can play a significant role in the SEB of glaciers (e.g. Sicart et al., 2008; Anderson et al., 2007; Gillett and Cullen, 2011) but the fluxes are poorly quantified, since they are usually evaluated using the so-called bulk aerodynamic (BA) method, based on the assumptions that fluxes are constant with height and that turbulent mixing scales with mean vertical gradients of wind speed, temperature and humidity near the surface. These assumptions are frequently violated over mountain glaciers. This is mainly due to frequent occurrence of katabatic winds (Poulos and Zhong, 2008) and to non-stationarity induced by the interaction of outer-layer turbulent structures with the surface flow. Such structures might be generated when synoptic forcing is strong and the large-scale atmospheric flow interacts with the complex orography (Smeets et al., 1999, 2000). Unmet similarity assumptions may lead to underestimating the flux with the BA method (Mahrt, 2008; Litt et al., 2015a). The impact of biased turbulent heat fluxes estimates on SEB calculations has been documented for vegetation canopies (Gellens-Meulenberghs, 2005; Stoy et al., 2013), but few studies have dealt with glacier or snow surfaces (e.g. Helgason and Pomeroy, 2012; Conway and Cullen, 2013). Evaluating the accuracy of the BA method for different large-scale forcings is necessary to understand the impact of the similarity assumptions on SEB calculations over mountain glaciers, and thus, on the evaluation of glacier melt rates from meteorological measurements or from climate data.

This study on the Saint-Sorlin glacier (French Alps, Grandes Rousses massif, 45° N, 6.1° E) compares turbulent flux measurements with observed large-scale weather patterns over Europe. We investigated the impact of turbulent flux measurement errors on glacier SEB calculations, for different prevailing atmospheric circulation patterns. The study covers two melt periods during the summers of 2006 and 2009, for which dominant atmospheric conditions were contrasted. Atmospheric circulation patterns were characterized with a daily time series of weather patterns derived from the analysis of Garavaglia et al. (2010). Surface-layer flow and turbulence data were obtained from two field campaigns deployed in the ablation area of the glacier. We used data from a 6-m mast measuring vertical profiles of wind speed and temperature, a high frequency Eddy-Covariance system, and radiation, temperature, wind speed and humidity measured by automatic weather stations. We characterized the turbulence in the surface-layer over the glacier and calculated the turbulent fluxes with both the BA and EC methods. We used these fluxes together with the measured radiative fluxes to compute the SEB. We discuss the difference on the SEB calculations resulting from the use of different methods to derive the turbulent fluxes, for the two melt periods.

The Cryosphere Discuss., doi:10.5194/tc-2016-93, 2016
Manuscript under review for journal The Cryosphere
Published: 13 May 2016

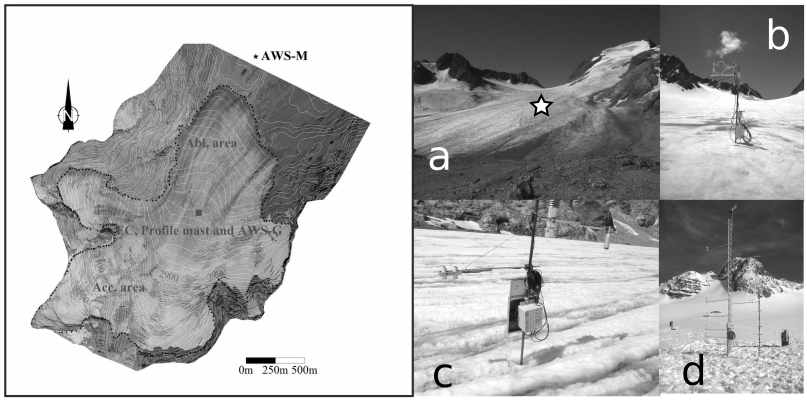

Figure 1. Overview of the glacier and the instruments installed during the field campaigns. (left) Topographic map of the glacier and position of the instruments. (a) Picture of the Saint-Sorlin glacier taken from the AWS-M (heading to the top of the glacier, south is at the horizon), (b-c-d) the instruments installed during the 2006 and 2009 campaigns.

2 Site and data

2.1 Saint-Sorlin glacier

Saint-Sorlin Glacier is a small mountain glacier (surface area $\simeq$3 km^2.) which altitude ranges between 2700 and 3400 m a.s.l (Fig. 1). It is located in the western part of the French Alps in the Grandes-Rousses massif (Fig. 2). It is characterized by a large flat ablation area (slope $\simeq 5°$) between 2700 and 2900 m a.s.l. Some steep slopes ($> 35°$) are found higher. Ice flows from the South-South-West to the North-North-East, inside a valley which has the same orientation. This valley is bordered by a steep ridge on its western flank and is opened on its eastern flank. The annual mass balance of the glacier has been monitored since 1957 (Vincent et al., 2000; Six and Vincent, 2014). All mass-balance data are available at http://www-lgge.obs.ujf-grenoble.fr/ServiceObs/index.htm.

2.2 Field campaigns

We used data from two field campaigns focussed on the ablation area of the glacier at around 2800 m a.s.l (Fig. 1). The first campaign was undertaken between 9 July and 28 August 2006, featuring a tower-mounted EC system measuring the three wind-speed components, air temperature and specific humidity at 20 Hz. The second campaign was staged between 13 June and 04 September 2009. We installed 5 cup anemometers and 9 ventilated thermocouples on a 6-m mast, measuring mean temperature and wind-speed profiles. During both campaigns there was an adjacent automatic weather station (AWS-G) consisting of instruments measuring mean aspirated air temperature and humidity, mean wind speed and direction, incoming and outgoing shortwave and longwave radiation fluxes. All masts were fixed into the ice. Height changes due to melt or snow deposition were measured with a sonic height ranger. Due to high melt rates ($\simeq$ 6 cm day^{-1}), the height of the sensors changed with time.

The Cryosphere Discuss., doi:10.5194/tc-2016-93, 2016
Manuscript under review for journal The Cryosphere
Published: 13 May 2016

Table 1. Characteristics of sensors from the automatic weather stations (AWS-G and AWS-M), the eddy-covariance (EC) and the profile mast. We present the random errors on the measurements, as provided by the manufacturer and the random measurement errors that we used to quantify uncertainties on the turbulent fluxes.

Quantity	Instrument	Precision according to the manufacturer	Accuracy used in this study	Mean sensor Height (m)
Profile Mast (2009 campaign)				
Aspirated air temperature, °C	Type-T thermocouple	0.1 °C	0.1 °C	0.74, 0.84, 1.04, 1.24, 1.54, 1.84, 2.44, 3.14, 4.64
Wind speed, m s^{-1}	Vector A100L2	1% of reading	0.1 m s^{-1}	0.83, 1.43, 2.33, 3.03, 4.03
Eddy Covariance System (2006 campaign)				
High frequency wind speed components, m s^{-1}	Campbell C-SAT3	w: ±0.040 m s^{-1} u, v: ±0.015 m s^{-1}	< ± 0.04 m s^{-1} ±0.015 m s^{-1}	2.37
High frequency sonic temperature, °C	Campbell C-SAT3	0.025°C	0.025°C	2.37
High frequency specific humidity, %	LICOR7500	2% of reading	2% of reading	2.37
Automatic Weather Stations (2006 and 2009 campaigns)				
Aspirated air temperature, °C and relative humidity, %	Vaisala HMP45C	±0.2 °C 3%	±0.2 °C 3%	1.8
Wind speed, m s^{-1}	Young 05103	0.3 m s^{-1}	0.3 m s^{-1}	2.50
Wind direction, deg	Young 05103	±3°	±3°	2.50
Incident and reflected shortwave radiation, Wm^{-2}	Kipp and Zonen CM3	10% on daily sums	0.4% 0.4%	1.20
Incoming and outgoing longwave radiation, Wm^{-2}	Kipp and Zonen CG3	10% on daily sums	0.4% 0.4%	1.20
Surface elevation changes, m	Campbell SR50	± 0.01 m	± 0.1 m	1.20

Instruments were manually lowered every 10 to 15 days. A picture of the instruments installed on the glacier is shown in Fig. 1. We also used data from an automatic weather station located outside the glacier (AWS-M), on a nearby moraine north of the site (1.5 Km), measuring the same variables as the AWS-G. This station is operated in the framework of the GLACIOCLIM program (les GLACIers, un Observatoire du Climat) that undergoes a follow-up of glaciers mass balance and meteorology in order to understand glacier fluctuations in terms of climatic variations. Table 1 summarizes all the instruments used and their characteristics.

The Cryosphere Discuss., doi:10.5194/tc-2016-93, 2016
Manuscript under review for journal The Cryosphere
Published: 13 May 2016

At the beginning of both campaigns, the glacier surface was covered with old winter or spring snow and was smooth (Fig. 1b and d). The glacier surface was irregular at the end of the campaigns due to strong melt that caused the apparition of gullies (Fig. 1a and c). Height changes of about 20 to 30 cm were observed on horizontal scales of about 2-3 m (not shown).

2.3 Data processing

Data have been processed in a similar way than in Litt et al. (2015b). All data were split into 1-h runs. High frequency data from the EC system were checked for quality (Vickers and Mahrt, 1997). Problems were mainly related to precipitation events or frost on the sensor heads. Bad quality runs were discarded (30%). Remaining good-quality runs were despiked (Vickers and Mahrt, 1997). A planar-fit rotation (Wilckzak et al., 2001) was applied on each 10 to 15 day period between field visits when they were manually lowered. From this rotation we derived the longitudinal (u), lateral (v) and vertical (w) wind-speed components. The sonic temperature was corrected for water vapour influences (Schotanus et al., 1983). The instrument heights were derived from the sonic height ranger and regular field visits and controls.

3 Methods

3.1 Characterization of large-scale forcing

We characterized the large-scale forcing and the frequency of typical atmospheric circulation patterns during the campaigns using a daily time series of weather patterns (WP). We used the Garavaglia et al. (2010) WP analysis which is based on the analysis of the shapes of the precipitation fields measured in the south-east of France, between 1956 and 1996. In this analysis, the shapes of the measured precipitation fields, at the daily time scale, are classified into 8 different classes. For each class, a mean observed geopotential field over Europe is computed. Then, for any day (inside or outside the period used to characterize the decomposition, e.g. 1956-1996) the observed geopotential field shape can be analysed and compared to the most similar mean geopotential field shape within the 8 fields proposed by the analysis, providing a WP.

A WP classification cannot be separated from the object it aims to characterize. An ideal WP decomposition for surface-layer turbulence studies would be based on surface energy flux-related variables such as ground-based measurements of temperature, wind speed or humidity rather than on precipitation. However, the Garavaglia et al. (2010) decomposition is useful here for an exploratory study, in which we use the WP to identify the direction and strength of the large-scale flows, and to obtain a frequency of typical large-scale circulation patterns during each campaign. Large-scale flow direction and strength is related to the displacement of low-pressure systems and thus to the shape of geopotential fields. Since each WP is associated with a mean geopotential field shape in the analysis of Garavaglia et al. (2010), it provides a simple and convenient tool for this study. An approximative direction of the atmospheric flow at low level above the ground can be associated with each WP (Fig. 2). In terms of wind regimes and meteorological conditions, the limitations of this WP analysis which is based on precipitation fields measured in the region of Saint-Sorlin glacier, are briefly discussed in Sect. 5.3.

The Cryosphere Discuss., doi:10.5194/tc-2016-93, 2016
Manuscript under review for journal The Cryosphere
Published: 13 May 2016

We grouped together the WP for which the wind conditions on the glacier were expected to be similar and we conserved three subsets. Low-pressure systems coming from the West, the South west and South can cause strong winds aligned with the valley and the glacier flow (Fig. 2). These conditions are related to Atlantic waves, South-west and South Circulations and Central Depressions. We grouped together the corresponding WP (patterns 1, 3, 4 and 7, Garavaglia et al., 2010) in a Strong Forcing (SF) subset. Large-scale flows associated with WP1 are not well aligned with the glacier (Fig. 2). Nevertheless for this WP we observe strong downslope flows above the glacier. We refer to weak large-scale flows, related to the presence of high-pressure systems (WP8) as Weak Forcing (WF). The WP 2, 5 and 6 are associated with Steady Oceanic Circulations, East Returns and North-east Circulations, respectively, and are grouped together as Other Forcing (OF). They present very distinct characteristics in terms of large-scale flow directions. They are generally associated with bad weather conditions, low wind speeds and erratic wind directions on the glacier, thus only a small fraction of the corresponding runs are classified as good-quality runs (Table 3) and we do not analyze them in detail herein.

3.2 Turbulence characteristics of the surface flow

High-frequency measurements were undertaken at low height (∼2 m), supposedly inside the surface layer, which is defined as the layer of air above the surface for which the turbulent fluxes do not change by more than 10% of their surface values (Stull, 1988). Monin-Obukhov similarity theory (herein, MOS, Monin and Obukhov, 1954), which underlies the BA method, assumes that the production of turbulent kinetic energy (TKE) in the stable surface layer is related to the mean local shear. The production of turbulence must be balanced by buoyancy and by destruction by viscous dissipation. No turbulent energy must be transported from the outer layers towards the surface layer and no advection shall transfer turbulence from some other parts of the field (Monin and Obukhov, 1954). To assess this issue, we computed the mean TKE ($\overline{e}$) using the EC data (overlines indicate temporal averages over a 1-h run and primes denote fluctuations around this mean):

$$\overline{e} = \frac{1}{2}\left(\overline{u'^2} + \overline{v'^2} + \overline{w'^2}\right), \quad (1)$$

with u, v and w the longitudinal, lateral and vertical wind speed components, respectively. We study the change of the TKE with the temperature gradients and the mean wind speed measured in the surface layer.

We studied the Fourier spectra (S) of the wind-speed components and the cospectra (Co) of u with w (associated with turbulent momentum flux) and of w with the potential temperature, θ (sensible heat), and with the specific humidity, q (latent heat). Following Smeets et al. (1999), individual spectra were normalized by the variance of w which led to a collapse of individual curves at high frequency. Heat flux-related cospectra were normalized by the kinematic flux ($\overline{w'\theta'}$ or $\overline{w'q'}$). We did not normalize Co_{uw} since $\overline{u'w'}$ is expected to be small and erratic near a wind-speed maximum as observed in katabatic flows. Medians of spectral powers over subsets of runs were calculated on equally spaced logarithmic intervals. Spectral analysis permitted a characterization of the turbulent flows. We used it to assess the validity of MOS, assuming that in an equilibrium surface layer, turbulent spectra and cospectra should compare well with the Kansas curves (Kaimal et al., 1972) measured under ideal conditions, and deviations from these curves are expected if the surface layer is not in equilibrium.

The Cryosphere Discuss., doi:10.5194/tc-2016-93, 2016
Manuscript under review for journal The Cryosphere
Published: 13 May 2016

The turbulent fluxes of sensible (H) and latent heat (LE) can be written as:

$$H = -\rho C_p \overline{w'\theta'}_s = -\rho C_p u_* T_*, \tag{2}$$

$$LE = -\rho L_e \overline{w'q'}_s = -\rho L_e u_* q_*, \tag{3}$$

where fluxes directed towards the surface and towards the atmosphere are defined as positive and negative, respectively. The symbols u_*, θ_* and q_* stand for turbulent velocity, temperature and humidity surface-layer scales. The subscript s refers to surface values, ρ is the air density ($kg\ m^{-3}$), C_p is the specific heat of humid air (1003.5 $J\ kg^{-1}\ K^{-1}$), L_e is the latent heat of sublimation of the ice ($2.83 \times 10^6\ J\ kg^{-1}$) when the surface is below freezing and the latent heat of vaporization (2.50×10^6 $J\ kg^{-1}$) when the surface is melting and k is the von-Karman constant (0.4). To apply Equations 2 and 3 we used alternately the BA and the EC methods (subscript b and EC refer to the BA or the EC method, respectively). The EC method relies on direct measurements of the fluctuating quantities u, θ and q, at some height above the surface, assuming fluxes are constant between the surface and this level. The BA method estimates u_*, θ_* and q_* using finite differences of mean measurements between the sensors and the surface, assuming that the fluxes scale with the mean vertical gradients:

$$u_{*_b} = k \frac{\overline{u}}{\left(\ln\left(\frac{z}{z_0}\right) - \psi_m\left(\frac{z}{L_*}\right)\right)} \tag{4}$$

$$\theta_{*_b} = k \frac{(\overline{\theta} - \overline{\theta}_s)}{\left(\ln\left(\frac{z}{z_t}\right) - \psi_t\left(\frac{z}{L_*}\right)\right)} \tag{5}$$

$$q_{*b} = k \frac{(\overline{q} - \overline{q}_s)}{\left(\ln\left(\frac{z}{z_q}\right) - \psi_q\left(\frac{z}{L_*}\right)\right)} \tag{6}$$

The length scales z_0, z_t and z_q are the dynamical, thermal and humidity roughness lengths (m), respectively. They were evaluated by least square iterative fitting of the temperature and wind speed vertical profiles measured in 2009, and assuming $z_q = z_t$ (e.g. Andreas, 2002; Sicart et al., 2014). We found as median values, $z_0 \simeq 0.001$ m and $z_t \simeq 0.00001$ m. Roughness lengths did not change significantly during the 2009 campaign, in spite of snow melt that uncovered the ice surface or caused the apparition of gullies, or with the occurrence of snow falls, probably because the uncertainties were larger than the actual changes (Sicart et al., 2014). Also, roughness lengths on glaciers depend mainly on the small scale features of the surface rather than on the size of large hummocky structures (Smeets and Van den Broeke, 2008). The state of the surface was similar in 2006 and 2009, and we use the same values for the roughness lengths for both field campaigns. In many studies, in order for the SEB to match the measured ablation, turbulent fluxes are adjusted using an effective roughness length z_e such as $z_0 = z_t = z_q = z_e$.

The Cryosphere Discuss., doi:10.5194/tc-2016-93, 2016
Manuscript under review for journal The Cryosphere
Published: 13 May 2016

This z_e is often larger than the actual aerodynamic values of the roughness lengths (Wagnon et al., 2003; Favier et al., 2004; Cullen et al., 2007; Six et al., 2009). We also computed the BA fluxes using an effective roughness parameter. We set z_e to 0.001 m, calibrated in Six et al. (2009) so that the SEB matches the observed melt during the 2006 campaign. Stability corrections $\psi_{m,h,q}$, for (m) momentum, (h) temperature and (q) humidity, respectively, were taken from Businger et al. (1971) and Dyer (1974). Temperature of the surface was derived from the outgoing longwave radiation measured at the AWS-G, assuming an emissivity of 0.99 for the ice or snow. Melt was observed most of the time, so that surface temperature was generally 0°C. The value of q_s was derived from the surface temperature assuming air at the surface was saturated. The length scale L_* is the Obukhov length defined as:

$$L_* = -\frac{\overline{\theta} u_*^2}{kg\theta_*} \tag{7}$$

The adimensional z/L_* is a scaling parameter in the surface layer. When evaluated with the BA method, this parameter documents the stability of the layer of air between the surface and the sensor assuming TKE production scales only on the mean local vertical gradients of wind speed and temperature. The evaluation of Equations 4, 5 and 6 requires an iterative scheme. A first evaluation of u_{*_b}, θ_{*_b} and q_{*b} was obtained assuming neutral stability ($z/L_{*b} = 0$). These estimates were used to compute a value of z/L_{*b}, which was used to calculate a new estimation of u_{*_b}, θ_{*_b} and q_{*b}, and so on, until convergence was reached.

We evaluated the random errors on the turbulent fluxes following the methods that Litt et al. (2015a) applied on the Zongo glacier. For the BA method, an analytical calculation was performed, propagating the uncertainties in the measurements of the meteorological variables (Table 1) through Equations 2 and 3. We assumed the uncertainties on the roughness lengths were $\delta \ln z_{0,t,q} \simeq 1.5$, following Sicart et al. (2014). We assumed the errors on the individual measurements were independent and that stability functions did not change much under small variations of the measurements. For the EC method, we assumed most random errors were due to a poor statistical sampling of the largest eddies (Vickers and Mahrt, 1997) and applied the Mann and Lenschow (1994) method which relates the random error to the time scale τ of the largest eddies of the flow. This timescale was derived from the peaks of the cospectra of w with θ and q obtained by Fourier analysis (Wyngaard, 1973).

3.3 Surface energy balance and melt

The melt rate was derived from the surface height changes measured with the SR50 sonic height ranger (h). We assumed the ice density was 900 kg m^{-3}. At the beginning of the campaigns, old snow was present at the surface, with measured density of 480 kg m^{-3}. The precipitated water equivalent during occasional snowfalls on the glacier were obtained from SAFRAN reanalysis data (Durand et al., 1993). The SEB was compared to the melt energy (Melt_i) derived from surface height (h) changes:

$$\mathrm{SEB} = \sum_{day} (SW_{inc} - SW_{out} + LW_{inc} - LW_{out} + H + LE) \tag{8}$$

The Cryosphere Discuss., doi:10.5194/tc-2016-93, 2016
Manuscript under review for journal The Cryosphere
Published: 13 May 2016

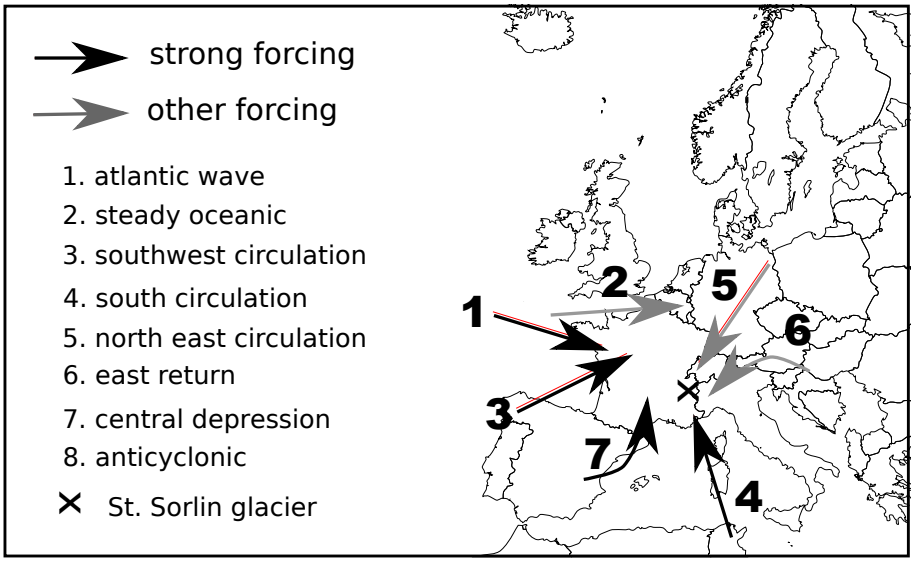

Figure 2. Direction of the atmospheric flow in the lower atmospheric layers for different WP (adapted from Garavaglia et al., 2010). (black arrows) Direction of the flow for the WP associated with SF and (grey arrows) direction of the flow for the other WP. No flow direction is shown for WF conditions (WP8) since atmospheric wind speed was weak and direction ill-defined for these conditions.

$$\mathrm{Melt}_i = (h(i+1) - h(i)) \times \rho_s L_f \tag{9}$$

Where i is a daily index, ρ_s is the density of the underlying snow or ice surface (kg m^{-3}), L_f is the latent heat of fusion of ice (3.34×10^5 J kg^{-1}). The symbol SW (resp. LW) stands for hourly mean shortwave radiation (respectively longwave). The subscript inc (respectively out) stands for incoming radiation (resp. outgoing). Sub-surface conductive heat flux was neglected because the surface remained close to melting day and night ($T_s > -3$°C). A simulation of the conduction flux below the snow or ice surface, using the surface temperature as the only input data, showed that this flux was negligible, even when surface temperature fell below zero during short periods of a few hours. The rare events of strong surface cooling, with surface temperature reaching ~ -11°C during the night, were associated with bad weather for which meteorological data quality was low due to frost or snow deposition on the sensors, these periods were discarded by the quality check procedure. We neglected the energy gains due to precipitation. Turbulent fluxes were obtained from the BA method with the roughness lengths z_0, z_t and z_q or the effective roughness z_e or from the EC method. All fluxes are expressed in W m^{-2}.

The Cryosphere Discuss., doi:10.5194/tc-2016-93, 2016
Manuscript under review for journal The Cryosphere
Published: 13 May 2016

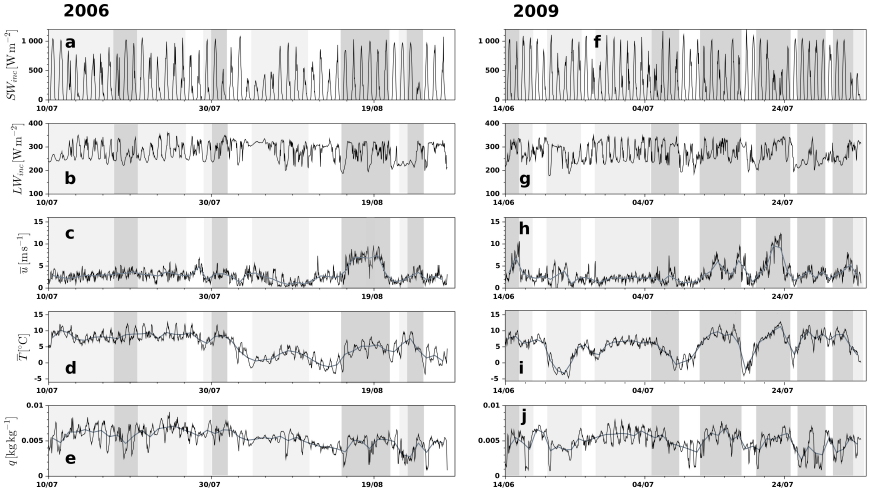

Figure 3. Change of the meteorological variables in the ablation zone of the glacier at the AWS-G in (left) 2006 and (right) 2009. (a-f) incoming shortwave radiation, (b-g) incoming longwave radiation, (c-h) wind speed, (d-i) air temperature and (e-j) specific humidity of the air. SF conditions are dark shaded and WF conditions are light shaded. The gray lines in lower panels (c, d, e, h. i and j) show daily averages.

4 Results

4.1 Meteorology and wind regimes

4.1.1 Meteorology

We describe the meteorological conditions of each campaign in terms of frequency of SF and WF conditions (Fig. 3). During the 2006 campaign, in July, the weather was often influenced by WF conditions (47 % of the time, Table 2), and to a lesser extent by SF conditions (26 %). During the long WF event at the beginning of the campaign, mean temperatures were high (8.2°C on average). The sky was generally clear, as shown by the values of SW_{inc} (> 500 W m^{-2}), but clouds were often developing in the afternoon (Six et al., 2009), as shown by the increases in LW_{inc} above 300 W m^{-2} and the peaks in the values of q. Wind speed was moderate (3 to 5 m s^{-1}) and the air was dry. In the beginning of August, during the 7-day WF event, the conditions were quite different than during the WF event of July. The high pressure systems were probably favouring the displacement of cold and humid air masses from Northern Europe, since temperature was low (0-5 °C), the sky covered (as visualized by frequent values of $SW_{inc} < 500$ W m^{-2}), and snow fall occurred on 03 August. During this period wind speed was low (2-3 m s^{-1}). The following sequences of SF were associated with high wind speeds (> 7 m s^{-1}), temperatures around 5 °C, and generally cloud covered conditions ($LW_{inc} \simeq 300$ W m^{-2}).

During the 2009 campaign, the WP frequencies were quite distinct from that of 2006: WF conditions prevailed from the beginning of the campaign until the end of June, but SF conditions prevailed during July and the beginning of August. 46% of the time of the campaign was characterized by SF conditions, and only 32% by WF conditions (Table 2). Similarly to the 2006

The Cryosphere Discuss., doi:10.5194/tc-2016-93, 2016
Manuscript under review for journal The Cryosphere
Published: 13 May 2016

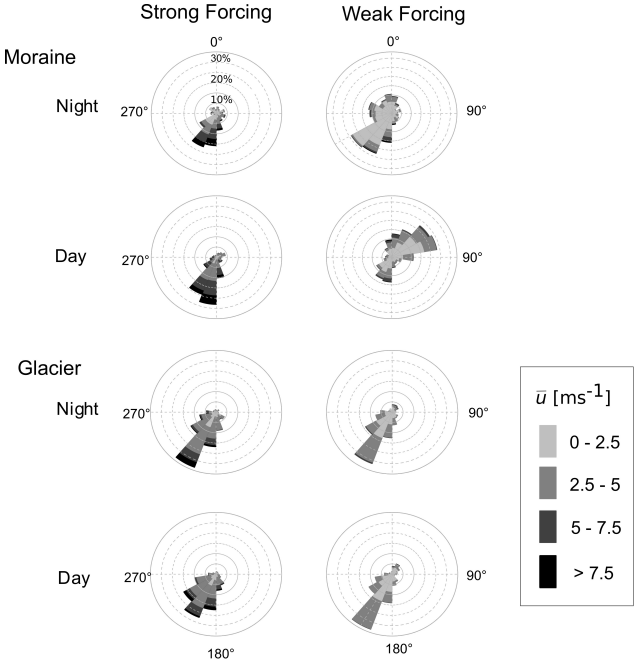

Figure 4. Rose diagrams of wind direction and speed measured by the AWS-G and the AWS-M for Strong (left panels) and Weak (right panels) Forcing conditions during the night (upper panels) and during the day (lower panels) .

campaign, two types of WF conditions were observed. One type (observed between 16 June and 18 June and between 27 June and 05 July) was characterized by temperatures above 5 °C and clear skies in the morning followed by cloudy conditions in the afternoons (see the peaks in LW_{inc} and q). The other type of WF (observed between 10 June and 25 June) was characterized by cold (-4 to 5 °C) and humid air, low to moderate wind speeds (<5 m s^{-1}), and cloudy skies. This event was similar to the August 2006 cold WF event. High wind speeds were observed for the SF conditions (from 5 to 12 m s^{-1}), and clouds were also frequently observed. Strong forcing conditions were characterized by warmer air in 2009 than in 2006 (Table 2).

4.1.2 Wind regimes

We defined the SF conditions as those related to low-pressure atmospheric systems that were associated with West, South-west or South circulations, roughly aligned with the glacier flow and with the valley. As a result, in the vicinity of the glacier, these conditions were associated with the largest wind speeds, and they seemed to trigger a dominant down-valley circulation, overwhelming convective circulations: on the glacier, wind was blowing downslope 99% of the time (Fig. 4). Day and night, the wind direction was similar over the glacier and outside the glacier. The median wind-speed profiles were nearly logarithmic below 2 m, and the temperature inversion was marked (Fig. 5). A katabatic wind-speed maximum was not frequently observed at low heights (Table 2 and Fig. 5), probably because it was located above the mast, or hidden in the background flow. The TKE was generally high (Table 2) for these conditions.

The Cryosphere Discuss., doi:10.5194/tc-2016-93, 2016
Manuscript under review for journal The Cryosphere
Published: 13 May 2016

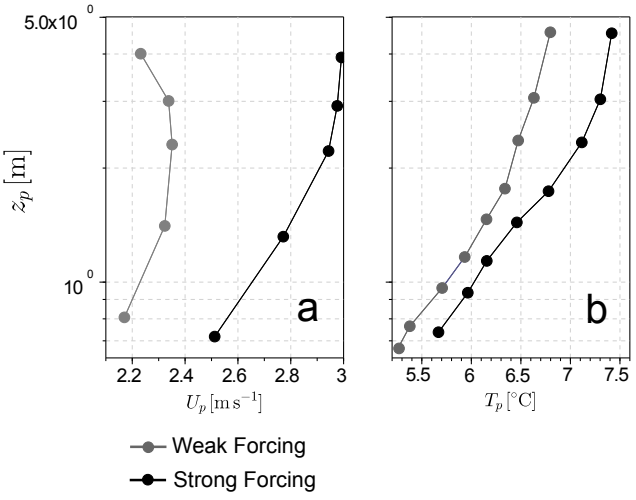

Figure 5. (a) Median wind-speed profiles and (b) temperature profiles during the 2009 field campaign for (gray) WF conditions and (black) SF conditions.

For WF conditions, associated with high-pressure systems and to weak synoptic forcing, the valley circulation seemed controlled by local thermal effects. On the glacier, wind blew mostly downslope, day and night (Fig. 4). Upslope winds were observed only 5% of the time. Over the glacier, the local katabatic forcing was dominant: a weak wind-speed maximum was observed at low heights ($\sim$ 2 m s^{-1} at $\sim$ 2 m, Fig. 5) for $\sim$ 70% of the WF situations (Table 2). During the day, convection probably drove the circulation in the valley: outside the glacier, the wind blew down the valley during the night and up the valley during the day (Fig. 4). Turbulent kinetic energy was generally small in these situations (Table 2).

4.1.3 Melt rates

During the 2006 campaign, melt rates as large as 6 cm day^{-1} were observed. Melt rates decreased after small snow events, since fresh snow significantly increased the surface albedo. Melt rates increased again a after a few days. Melt was not observed by the sounding height ranger after 20 August. After this date, we observed a very irregular glacier surface (Sect. 2.2). The total measured melt was 1.55 m.w.eq. During the 2009 campaign, melt rates were slightly lower than in 2006 (3-4 cm day^{-1}) at the beginning of the campaign, since large amounts of old winter or spring snow, of larger albedo than ice, were still present on the glacier surface in June. Larger melt rates were observed after 15 July, when the ice was uncovered. Melt rates were dampened by snow fall around 19 July, and then increased again after a few days. The surface was chaotic after this date (Sect. 2.2). The total measured melt was 2.20 m.w.eq.

The Cryosphere Discuss., doi:10.5194/tc-2016-93, 2016
Manuscript under review for journal The Cryosphere
Published: 13 May 2016

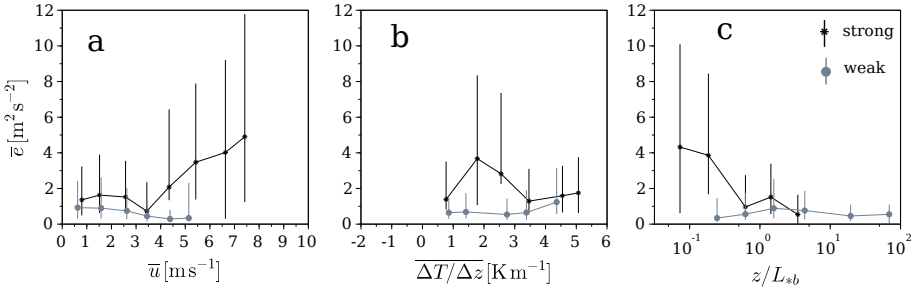

Figure 6. Change of TKE measured with the EC system during the 2006 campaign (a) with the mean wind speed, (b) with the mean temperature gradient and (c) with z/L_{*b} derived from the bulk aerodynamic method. Bin-median values are presented and vertical bars indicate the interquartile range.

4.2 Turbulent characteristics of the surface flow

4.2.1 Turbulent kinetic energy

For WF cases, the TKE was not related to the mean wind speed in the surface layer (Fig. 6a), nor with the strength of the temperature inversion (Fig. 6b). The surface layer was generally stable (Fig. 6c). For SF conditions the TKE increased with increasing wind speed (Fig. 6a). High TKE values were associated with a less marked thermal stratification (Fig. 6b), and near-neutral stability conditions (Fig. 6c). For both SF and WF conditions, for low TKE, the surface layer was stable and the TKE did not relate to the wind speed. For high TKE, the TKE was somewhat related to the mean wind speed and the surface-layer was near-neutral.

For WF (resp. SF) conditions, TKE generally was low (resp. high). However, some high (resp. low) TKE cases remained in the classification (Table 2 and Fig. 6). We thus characterized the surface layer flow by selecting 2 subsets of runs of the EC data of 2006 that exhibited contrasted TKE range. We analysed the most frequent runs for which wind blew downslope (direction between 90° and 270°, 85 % of the GQR), keeping only cases for which $H_{EC} < -5$ W m^{-2} and $\overline{u} > 2$ m s^{-1} in order to filter for cases when turbulence was sufficiently developed. We separated these runs in two subsets, one for which TKE was high, requiring $\overline{e} > 2$ m^2 s^{-2} (14% of the GQR) and a subset for which TKE was low, with $\overline{e} < 1$ m^2 s^{-2} (31% of the GQR). This classification distinguishes typical turbulent conditions and groups together spectra and cospectra of similar shapes (Sect. 4.2.2). Note that 52% of SF conditions show $\overline{e} > 2$ m^2 s^{-2} and 67 % of the WF conditions show $\overline{e} < 1$ m^2 s^{-2}.

4.2.2 Spectral analysis

The Fourier analysis of the 2006 EC data showed that the horizontal and the vertical wind speed oscillated at low frequency, more than expected for an equilibrium surface layer (Fig. 7a and 7b). For $n < 10^{-1}$ the horizontal and vertical wind-speed spectra were higher than the prediction of Kaimal et al. (1972) for the z/L_* measured with the BA method in the surface layer. The amplitude of these low-frequency oscillations was much larger for the longitudinal than for the vertical wind speed.

The Cryosphere Discuss., doi:10.5194/tc-2016-93, 2016
Manuscript under review for journal The Cryosphere
Published: 13 May 2016

Similar observations were made for large and low TKE runs, except that the peak in S_u was observed at $n \sim 5 \times 10^{-2}$ and $n \sim 5 \times 10^{-3}$ when $\overline{e}$ was high and low, respectively.

The low-frequency oscillations of u and w affected the momentum flux. For high $\overline{e}$ and $n > 10^{-2}$ the median cospectrum of w with u was negative (Fig. 7d). For $n < 10^{-2}$ the median cospectrum reversed its sign, a peak was observed at the same frequency as the low-frequency peak of S_u ($n \sim 5 \times 10^{-2}$), and the dispersion between the individual cospectra was large. When $\overline{e}$ was low, Co_{uw} was low too. For $n > 10^{-2}$ the median cospectrum was slightly positive, indicating an upward momentum flux, probably due to the presence of a katabatic wind-speed maximum just below the sensor, roughly at 2 m above the ground (Fig. 5). For $n < 10^{-2}$ the median cospectra was low, but the individual cospectra were dispersed around zero (hardly visible in Fig. 7d)

Low-frequency oscillations also influenced the sensible (Fig. 7c) and the latent heat fluxes (not shown). When $\overline{e}$ was high, all the individual cospectrum collapsed well and the dispersion was low. The median cospectrum exhibited a small plateau at the frequency of the peak in the Kaimal curve. A peak was observed above the Kaimal curve at $n \sim 5 \times 10^{-1}$. For $n < 5 \times 10^{-1}$, the median cospectrum fell to zero. When $\overline{e}$ was low, the dispersion between the individual cospectra was high. The median cospectrum peaked at the frequency of the peak in the Kaimal curve ($n \sim 5 \times 10^{-1}$). For $n < 5 \times 10^{-1}$ the median cospectra fell to zero erratically. At the lowest frequency end, individual cospectra were dispersed around zero.

4.2.3 Turbulent fluxes

During the 2006 campaign, the sensible heat flux was generally a gain of energy for the glacier (Fig. 8a). It was moderately positive (around 50 W m^{-2}) during July due to moderate wind speeds in prevailing anticyclonic WF conditions ($\sim$ 2.5 m s^{-1}, Table 2). The sensible heat flux was near zero at the beginning of August because the air was cold and wind was very low. It was significantly positive during the SF event between 15 July and 21 July, because of strong winds. Then moderate fluxes were observed. The latent heat flux was a small loss of energy for the glacier. It remained generally small in magnitude (>-30 W m^{-2}), since the water content in the air did not change significantly ($q \sim 0.005$, Table 2). Both negative (sublimation) and positive (condensation) were observed in July. Latent heat flux was near zero at the beginning of August, and it was strongly negative (~ -75 W m^{-2}) during the SF event between 15 August and 21 August, due to high wind speeds. After this event, it remained generally slightly negative.

During the 2009 campaign, the sensible heat flux was slightly positive in June and the first half of July, when the WF conditions prevailed ($u \sim 2.6$ m s^{-1}). It was strongly positive (Fig. 8b) only for the short SF event at the beginning of the campaign. During the second half of July, during SF events with large wind speeds ($\sim$5.5 m s^{-1}) associated with warm air (~ 9°C), the sensible heat flux was highly positive, especially between 20 and 25 July (> 200 W m^{-2}). The sensible heat fluxes were frequently larger than in 2006, due to more frequent SF conditions, for which wind speed was larger and air was warmer than for SF conditions in 2006. The latent heat flux generally remained small and negative, due to wet air, except during the SF event between 20 and 25 July for which it was highly negative, due to high wind speeds and dry air.

When TKE was low, the BA method based on the profile-derived roughness lengths and the EC method both provided similar fluxes, and they were smaller then when TKE was high (Table 2). When TKE was high, the EC-method mean net turbulent

The Cryosphere Discuss., doi:10.5194/tc-2016-93, 2016
Manuscript under review for journal The Cryosphere
Published: 13 May 2016

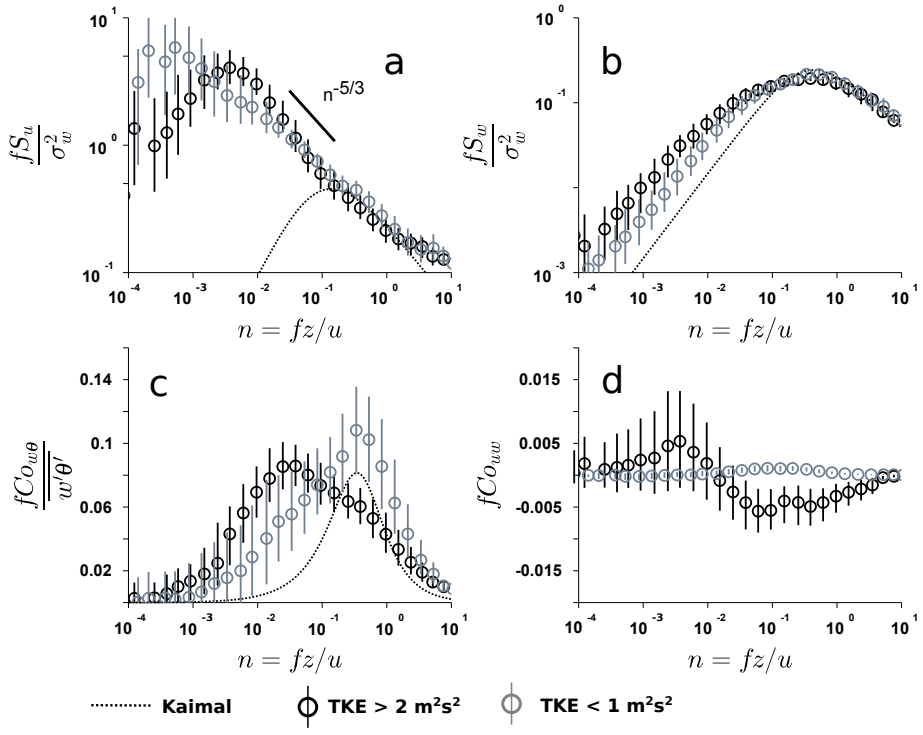

Figure 7. Fourier analysis of the high frequency EC data during the 2006 campaign. The median spectra and cospectra calculated over (black) the high TKE and (grey) the low TKE subsets are presented together with (black dotted) the Kaimal et al. (1972) curve. (circles) average of the spectra or cospectra over a bin of normalized frequency and (vertical bars) interquartile range of the spectra or cospectra over the same bin. (a) Spectra of longitudinal wind speed u, (b) spectra of w with θ, (c) cospectra of w with T and (d) cospectra of w with u.

fluxes ($H + LE$) were significantly larger than the BA method fluxes evaluated with the profile-derived roughness lengths. Random errors were too low to explain the discrepancy (not shown). Using an effective roughness length z_e in the BA method yielded net fluxes which were, on average, alike those of the EC method.

5 Discussion

5.1 Turbulence in the surface layer.

When the TKE was high, which was observed for 52% of SF conditions, the characteristics of the wind-speed spectra were similar to that of a surface layer influenced by outer-layer turbulence: the variance of u was strongly enhanced at low frequency compared to what is expected for an equilibrium surface layer, while a limited increase was observed in the w spectra, a combination of observations which agrees with the previsions of Högström et al. (2002) for surface layers disturbed by large eddies. In the vicinity of the surface, large-scale structures transported from the outer-layer, are supposedly elongated horizontally due to the surface blocking, and due to the large shear in the surface layer. As a result, they must induce large horizontal fluctua-

The Cryosphere Discuss., doi:10.5194/tc-2016-93, 2016
Manuscript under review for journal The Cryosphere
Published: 13 May 2016

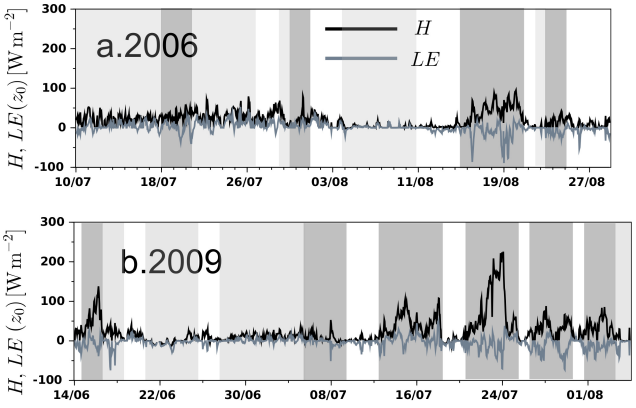

Figure 8. Change of the turbulent fluxes derived from the BA method and the profile-derived roughness lengths, during the (a) 2006 and (b) 2009 field campaigns. (black curve) The sensible heat fluxes and (grey curve) the latent heat fluxes are shown. The SF (resp. WF) conditions are dark-shaded (resp. light-shaded) in grey.

tions of the horizontal wind speed while the vertical wind speed must be less affected. Also, a $n^{-5/3}$ slope was observed on the low frequency part of the u spectra when TKE was large (Fig. 7a). This signature resembles that of an outer, well-mixed layer (Højstrup, 1982). Similar spectral shapes were observed over other mountain glaciers when synoptic forcing was strong (Smeets et al., 1999; Litt et al., 2015b). In these studies, the observed low-frequency oscillations were attributed to the interaction of large scale coherent structures with the surface-layer turbulence. Such structures can be generated when the large-scale flow interacts with the complex mountain orography. It is probable that these kinds of structures were influencing the surface flow on Saint-Sorlin glacier.

In these situations, the TKE transport term was probably not zero: significant TKE could be transported from the outer layer and the surface layer turbulence was not in equilibrium with local production, explaining why $\overline{e}$ did not exhibit a clear dependence on the mean temperature gradient and on the mean wind speed measured at low height in the surface layer (Fig. 6). Perturbations of the surface layer seemed to have a strong effect on the momentum flux, as shown by the cospectra of u and w, which exhibited erratic contributions around zero at low frequencies (Fig. 7). The perturbations also affected the turbulent heat fluxes, since the cospectra of w with θ peaked and contained more energy at low frequency than the Kaimal predictions. These perturbations likely originated from turbulent structures sharing similar time scales, since the low frequency peak was observed systematically at $n \sim 10^{-2}$. The influence of these structures on the fluxes was always of the same sign and induced larger heat fluxes magnitudes than predicted by the Kansas curve. The EC method probably accounted for this contribution, whereas the BA method could not take it into account because the turbulent mixing did not relate well to the mean gradients in the surface-layer (Litt et al., 2015b). This explains why the BA method systematically underestimated the fluxes in these conditions (Table 2). Random measurements errors in the EC method were mainly related to poor sampling of large-scale eddies. For the BA method the largest source of random error is the uncertainty on the roughness lengths, which were not

The Cryosphere Discuss., doi:10.5194/tc-2016-93, 2016
Manuscript under review for journal The Cryosphere
Published: 13 May 2016

precisely defined ($\delta \ln z_{0,t} = 1.5$, Litt et al., 2015a). Nevertheless, these errors were too low to explain the observed difference between the fluxes derived from each method.

When the TKE was small, which was observed for 68% of WF conditions, low-frequency oscillations of the wind speed were common, probably as a result of katabatic flow oscillations (McNider, 1982) and residual outer-layer perturbations. The cospectra of w with u was slightly positive (Fig. 7d), suggesting a wind maximum was present just below the EC system, in agreement with the profile measurements of the 2009 campaign for WF conditions (Fig. 5). A katabatic flow leads to vertical flux divergence (Denby and Greuell, 2000) and advection of heat and momentum from higher parts of the glacier. When the flow oscillated, the depth of the katabatic layer and the height of the wind-speed maximum probably oscillated too, which explains the erratic behaviour of the cospectra of w with θ at low frequencies (Fig. 7). The fluxes from the EC system, measured at 2 m, were decorrelated from the surface fluxes, probably because the fluctuating katabatic wind-speed maximum provoked an erratic divergence of the fluxes in the first meters above the surface. Probably the concept of a surface layer was not even relevant. As a result, the fluxes from the BA method and the EC method were decorrelated (not shown).

5.2 Surface energy balance and melt

During both campaigns, the SEB was mainly controlled by large radiative fluxes, regardless of large-scale forcing, but the contribution of turbulent fluxes to the SEB was significant (Fig. 9). Random errors on turbulent fluxes remained small in comparison with the total SEB. All SEB calculations compared well with the sonic height ranger measurements, assuming a $\pm 10\%$ relative error on the latter.

Weak forcing conditions dominated during the 2006 campaign (Table 2), and the mean net turbulent fluxes were moderate (~ 25 W m^{-2}). Since TKE was generally low for these conditions, small differences were observed between turbulent fluxes derived with different calculation methods, compared to the large radiative inputs (Fig. 9). In 2009 for these conditions, turbulent fluxes were nearly negligible (< 10 W m^{-2}), and the difference between them was too low in absolute terms to yield significant differences in the calculated SEB.

Since TKE was generally large in SF conditions, one would have expected the EC method to provide larger turbulent fluxes than the BA method (Sect. 4.2). Nevertheless, for SF conditions in 2006, all turbulent fluxes calculation methods provided similar mean fluxes (~ 35 W m^{-2}). This could be explained by the presence of low TKE runs in these conditions, for which the discrepancies between turbulent flux calculation methods were small. In 2009 for SF conditions, the difference between the SEB calculations was high (Fig. 9d), the z_e method providing stronger net turbulent fluxes (70 W m^{-2}) than the z_0 method (50 W m^{-2}). In 2009 the SF conditions were frequent and were characterized by warmer air and higher wind speeds than the SF conditions of 2006 (Table 2). Low-frequency oscillations, originating from large-scale orographic disturbances, probably transported TKE in the surface layer that did not scale with the mean vertical gradients. These situations favoured frequent large TKE conditions, which lead to an underestimation of the turbulent fluxes by the BA method (Sect. 4.2). Using an effective roughness length in the BA method provided larger fluxes than using the profile-derived roughnesses (Table 2). Though validation with EC measurements would be needed, this suggests that the use in SEB models of an effective roughness length, such as $z_e > z_0$, in order to increase the turbulent fluxes so that the SEB matches the melt, is actually a way to compensate

The Cryosphere Discuss., doi:10.5194/tc-2016-93, 2016
Manuscript under review for journal The Cryosphere
Published: 13 May 2016

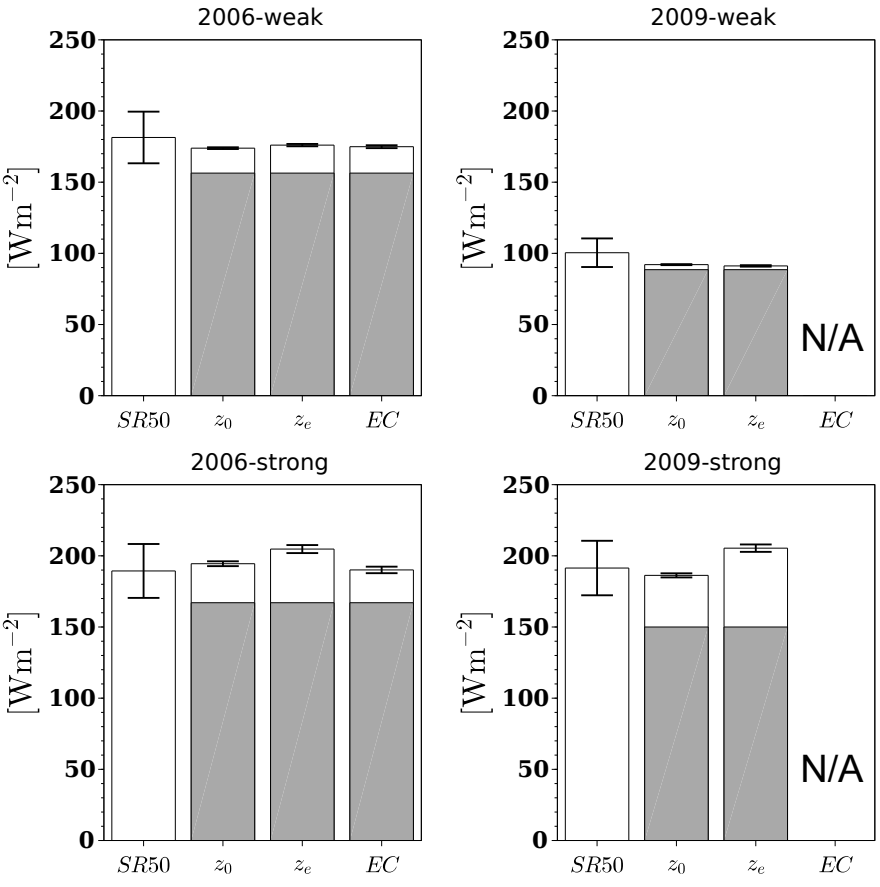

Figure 9. Mean measured melt and SEB for (a and b) WF and (c and d) SF conditions, during (a and c) 2006 and (b and d) 2009 campaigns. (gray) radiation balance, (white) melt measured by the SR50 or net turbulent flux ($H + LE$) evaluated with the BA method with profile-derived roughness (z_0), with the BA method with z_e and with the EC method. Random error on turbulent fluxes and a $\pm 10\%$ interval for the SR50 measurements are shown by the black error bars.

potential biases in the BA turbulent fluxes due to failure of the MOS when TKE is high. Nevertheless, both SEB estimates lie in the uncertainty range of the observed melt.

5.3 Weather patterns

The analysis of meteorological conditions and wind regimes shows that using the WP decomposition of Garavaglia et al. (2010) is only partly adapted for SEB studies. For WF conditions only one WP is used which is always associated with weak wind speeds on the glaciers, but for which temperature and cloud cover can be significantly different. The SF conditions are generally characterized by strong winds and cloud covered conditions on the glacier, but can be associated with either cold or warm air flows. However, the WP analysis is helpful in identifying different kind of circulations in the valley: for WF conditions local

The Cryosphere Discuss., doi:10.5194/tc-2016-93, 2016
Manuscript under review for journal The Cryosphere
Published: 13 May 2016

thermal wind such as katabatic flows drive the circulation whereas in SF the circulation is dominated by large-scale flows. It also provides a rough classification of the turbulence conditions in the glacier surface-layer, since SF and WF conditions are, in the glacier surface layer, likely associated with high and low TKE conditions, respectively.

6 Conclusions

During the summers of 2006 and 2009, field measurement campaigns were undertaken in the ablation zone of Saint-Sorlin Glacier, in the French Alps. We analysed Eddy-Covariance data from the 2006 campaign and temperature and wind-speed vertical profiles from the 2009 campaign. We characterized the wind regimes and associated surface-layer turbulent flows, in relation to the large scale forcing as characterized from the weather pattern decomposition of Garavaglia et al. (2010). We evaluated the turbulent fluxes with the bulk aerodynamic (BA) method using observed and melt-calibrated roughness parameters and the Eddy-Covariance (EC) method. We also calculated the surface energy balance and studied its changes in relation with weather patterns.

The sensible heat fluxes (H) were warming the surface, they were generally larger in magnitude than latent heat fluxes (LE) which were, on average, a small loss of energy for the glacier. When synoptic forcing was weak, local thermal effects drove the valley wind circulation. A katabatic wind-speed maximum was frequently observed at low height on the glacier (around 2 m, 71% of these conditions). The turbulent kinetic energy (TKE) was generally low (< 1 m^2 s^{-2}, 68% of the cases), and both H and LE remained small in magnitude. When synoptic forcing was strong, under the influence of low-pressure systems, the large-scale winds roughly aligned with the glacier flow and drove the wind circulation. High wind speeds were observed on the glacier, the TKE was generally high (> 2 m^2 s^{-2}, 52% of the cases) and the katabatic wind-speed maximum was not frequently observed below 5 m (<40% of the time). Sensible heat fluxes were high (>100 W m^{-2}) in these conditions, due to high wind speeds. The sublimation ($LE < 0$) magnitude increased only moderately since the air remained humid, and LE did not cancel the energy gain due to H, so the net flux ($H + LE$) was highly positive.

For all conditions, low-frequency oscillations were observed in the wind-speed signals. When TKE was low, as often observed for weak synoptic forcing, this was likely due to oscillations of the katabatic flow. When TKE was high, as frequently seen for strong synoptic forcing, this was likely due to large-scale orographic disturbances. The TKE did not scale with the mean temperature and wind-speed gradients in the surface layer, suggesting that TKE transport was non-negligible and that the surface layer turbulence was not in equilibrium with local turbulence production. These low-frequency oscillations influenced the turbulent momentum and heat fluxes in the surface layer. The non-equilibrium of the surface-layer led to erratic discrepancies between EC fluxes and BA fluxes when TKE was low. The mean turbulent fluxes calculated with both methods tended to be similar, since the differences between them compensated when averaged over several runs. A systematic underestimation of the EC fluxes by the BA fluxes was observed when TKE was large, which could not be attributed to random measurement errors. As a result the BA fluxes were significantly smaller in magnitude than the EC fluxes.

Surface energy balance calculations compared well to the observed melt. During the 2006 campaign, using turbulent fluxes from the BA or from the EC method did not provide significantly different results. The weather during that campaign was

dominated by anticyclonic circulations and weak large-scale forcing. Hence, the turbulent fluxes from both methods were small and not significantly different on average. During the 2009 campaign, many low-pressure systems, associated with strong and warm winds, were reported. The SEB calculated with profile-derived roughness parameters underestimated the SEB derived with effective roughnesses. Probably the BA method could not account for turbulent mixing that did not scale with the mean gradients in the surface layer. This suggests that in frequent warm and windy conditions, systematic biases might affect the SEB and may lead to underestimating the melt rate on alpine glaciers when the turbulent fluxes are evaluated with profile-derived roughnesses. The use of an effective roughness to calibrate the SEB on the observed melt increases the fluxes and thus can act as a correcting parameter.

Studies covering more melt periods are necessary to better understand how weather patterns relate to the different SEB terms and to better understand the links between large-scale forcing and mass balance in the vicinity of the glaciers, using dedicated variables to drive a weather pattern decomposition. This would help to understand the climatic processes governing inter-annual variations in the melt regimes of the glaciers. Furthermore, the potential turbulent flux biases might impact the total calculated melt significantly, when calculated over long periods. Turbulent flux error studies would be necessary on other glaciers where turbulent fluxes dominate the SEB (e.g. at high latitudes), to assess the effect of these potential biases on melt rate evaluation from climate data.

Acknowledgements. This work was funded by the French SO/SOERE GLACIOCLIM (http://www-lgge.ujf-grenoble.fr/ServiceObs/index.htm) and the ANR program TAG 05-JCJC-0135. We kindly thank EDF for providing the daily time series of WPs. We thank Romain Biron and Jean-Philipe Chazarin for the technical and field work, and Adrien Gilbert and Marion Reveillet for stimulating discussions.

The Cryosphere Discuss., doi:10.5194/tc-2016-93, 2016
Manuscript under review for journal The Cryosphere
Published: 13 May 2016

References

Anderson, B., Mackintosh, A., Stumm, D., George, L., Kerr, T., Winter-Billington, A., and Fitzimons, S.: Climate sensitivity of a high-precipitation glacier in New-Zealand, J. Glaciol., 56, 114–128(15), 2007.

Andreas, E.: Parameterizing Scalar Transfer over Snow and Ice: A Review., Jour. Hydrometeorol., 3, 417–432., 2002.

Businger, J. A., Wyngaard, J. C., Izumi, Y., and Bradley, E. F.: Flux-Profile Relationships in the Atmospheric Surface Layer, J. Atmos. Sci., 28, 181–189, 1971.

Conway, J. and Cullen, N.: Constraining turbulent heat flux parameterization over a temperate maritime glacier in New Zealand, Annals of Glaciology, 63, doi:10.3189/2012AoG63A604, 2013.

Corti, S., Molteni, F., and Palmer, T.: Signature of recent climate change in frequencies of natural atmospheric circulation regimes, Nature, 398, 799–802, 1999.

Cullen, N., Mölg, T., Kaser, G., Steffen, K., and Hardy, D.: Energy-balance model validation on the top of Kilimanjaro, Tanzania, using eddy covariance data., Annals of Glaciology, 46, 227–233, 2007.

Denby, B. and Greuell, W.: The use of bulk and profile methods for determining surface heat fluxes in the presence of glacier winds., Journal of Glaciology, 46, 445–452, 2000.

Durand, Y., Brun, E., Merindol, L., Guyomarc'h, G., Lesaffre, B., and Martin, E.: A meteorological estimation of relevant parameters for snow models, Annals of Glaciology, 18, 65–71, 1993.

Dyer, A.: A review of flux-profile relationships., Boundary-Layer Meteorol., 3, 363–372, 1974.

Favier, V., Wagnon, P., and Ribstein, P.: Glaciers of the outer and inner tropics: A different behaviour but a common response to climatic forcing, Geophys. Res. Lett., 31, L16 403, 2004.

Garavaglia, F., Gailhard, J., Paquet, E., Lang, M., Garçon, R., and Bernardara, P.: Introducing a rainfall compound distribution model based on weather patterns sub-sampling, Hydrol. Earth. Syst. Sc., 14, 951–964, 2010.

Gellens-Meulenberghs, F.: Sensitivity Tests of an Energy Balance Model to Choice of Stability Functions and Measurement Accuracy, Boundary-Layer Meteorol., 115, 453–471, 2005.

Gillett, S. and Cullen, N. J.: Atmospheric controls on summer ablation over Brewster Glacier, New Zealand, Int. J. Climatol., 31, 2033–2048, 2011.

Helgason, W. and Pomeroy, J.: Problems Closing the Energy Balance over a Homogeneous Snow Cover during Midwinter, J. Hydrometeorol., 13, 557–572, 2012.

Hock, R.: Temperature index melt modelling in mountain areas, Journal of Hydrology, 282, 104–115, 2003.

Højstrup, J.: Velocity Spectra in the Unstable Planetary Boundary Layer, J. Atmos. Sci., 39, 2239–2248, 1982.

Huss, M., Hock, R., Bauder, A., and Funk, M.: 100-year mass changes in the Swiss Alps linked to the Atlantic Multidecadal Oscillation, Geophysical Research Letters, 37, 2010.

Högström, U., Hunt, J. C. R., and Smedman, A. S.: Theory and Measurements for Turbulence Spectra and Variances in the Atmospheric Neutral Surface Layer., Boundary-Layer Meteorology, 103, 101–124, 2002.

Kaimal, J., Wyngaard, J., Izumi, Y., and Coté, O. R.: Spectral characteristics of surface-layer turbulence., Quart. J. Roy. Meteor. Soc., 417, 563–589, 1972.

Litt, M., Sicart, J. E., and Helgason, W. D.: A study of turbulent fluxes and their measurement errors for different wind regimes over the tropical Zongo glacier during the dry season., Atmos. Meas. Tech., 8, 3229–3250, 2015a.

Litt, M., Sicart, J. E., Helgason, W. D., and Wagnon, P.: Turbulence Characteristics in the Atmospheric Surface Layer for Different Wind Regimes over the Tropical Zongo Glacier (Bolivia, 16° S), Boundary-Layer Meteorol., pp. 1–25, doi:10.1007/s10546-014-9975-6, 2015b.

Mahrt, L.: Bulk formulation of surface fluxes extended to weak-wind stable conditions, Quart. J. Roy. Meteor. Soc., 134, 1–10, 2008.

Mann, J. and Lenschow, D. H.: Errors in airborne flux measurements, J. Geophys. Res., 99, 14 519–14 526, 1994.

McNider, R. T.: A Note on Velocity Fluctuations in Drainage Flows, J. Atmos. Sci., 39, 1658–1660, 1982.

Monin, A. and Obukhov, A.: Basic laws of turbulent mixing in the surface layer of the atmosphere, Tr. Akad. Nauk SSSR Geophiz. Inst., 24, 163–187, 1954.

Oke, T.: Boundary Layer Climates, 2nd ed., Routeledge, New York, 1987.

Pellicciotti, F., Buergi, C., Immerzeel, W. W., Konz, M., and Shrestha, A. B.: Challenges and Uncertainties in Hydrological Modelin of Remote Hindu Kush-Karakoram-Himalayan Basins: Suggestions for Calibration Strategies, Mountain Research And Development, 32, 39–50, 2012.

Poulos, G. and Zhong, S. S.: An Observational History of Small-Scale Katabatic Winds in Mid-Latitudes, Geography Compass, 2, 1798–1821, 2008.

Schotanus, P., Nieuwstadt, F., and Bruin, H.: Temperature measurement with a sonic anemometer and its application to heat and moisture fluxes, Boundary-Layer Meteorol., 26, 81–93, 1983.

Sicart, J., Hock, R., and Six, D.: Glacier melt, air temperature, and energy balance in different climates: The Bolivian Tropics, the French Alps, and northern Sweden, J. Geophys. Res., 113, D24 113, 2008.

Sicart, J. E., Litt, M., Helgason, W., Tahar, V. B., and Chaperon, T.: A study of the atmospheric surface layer and roughness lengths on the high-altitude tropical Zongo glacier, Bolivia, J. Geophys. Res. Atmos., 119, 3793–3808, 2014.

Six, D. and Vincent, C.: Sensitivity of mass balance and equilibrium-line altitude to climate change in the French Alps, Journal of Glaciology, 60, 867–878, 2014.

Six, D., Wagnon, P., Sicart, J., and Vincent, C.: Meteorological controls on snow and ice ablation for two contrasting months on Glacier de Saint-Sorlin, France, Ann. Glaciol., 50, 66–72, 2009.

Smeets, C., Duynkerke, P., and Vugts, H.: Observed wind profiles and turbulence fluxes over an ice surface with changing surface roughness, Boundary-Layer Meteorol., 92, 99–121, 1999.

Smeets, C., Duynkerke, P., and Vugts, H.: Turbulence characteristics of the stable boundary layer over a mid-latitude glacier. Part II: Pure katabatic forcing conditions, Boundary-layer Meteorol., pp. 73–107, 2000.

Smeets, C. J. P. P. and Van den Broeke, M. R.: Temporal and Spatial Variations of the Aerodynamic Roughness Length in the Ablation Zone of the Greenland Ice Sheet, Boundary-Layer Meteorol., 128, 315–338, 2008.

Stoy, P. C., Mauder, M., Foken, T., Marcolla, B., Boegh, E., Ibrom, A., Arain, M. A., Arneth, A., Aurela, M., Bernhofer, C., Cescatti, A., Dellwik, E., Duce, P., Gianelle, D., van Gorsel, E., Kiely, G., Knohl, A., Margolis, H., McCaughey, H., Merbold, L., Montagnani, L., Papale, D., Reichstein, M., Saunders, M., Serrano-Ortiz, P., Sottocornola, M., Spano, D., Vaccari, F., and Varlagin, A.: A data-driven analysis of energy balance closure across FLUXNET research sites: The role of landscape scale heterogeneity, Agric. For. Meteorol., 171-172, 137–152, 2013.

Stull, R.: An Introduction to Boundary Layer Meteorology, Springer, Netherlands, 1988.

Vickers, D. and Mahrt, L.: Quality Control and Flux Sampling Problems for Tower and Aircraft Data, J. Atmos. Oceanic Technol., 1, 512–526, 1997.

Vincent, C., Vallon, C., Reynaud, L., and Meur, E. L.: Dynamic behaviour analysis of glacier de Saint Sorlin, France, from 40 years of observations, 1957–97, Journal of Glaciology, 46, 499–506(8), 2000.

Viviroli, D., Archer, D. R., Buytaert, W., Fowler, H. J., Greenwood, G. B., Hamlet, A. F., Huang, Y., Koboltschnig, G., Litaor, M. I., López-Moreno, J. I., Lorentz, S., Schädler, B., Schreier, H., Schwaiger, K., Vuille, M., and Woods, R.: Climate change and mountain water resources: overview and recommendations for research, management and policy, Hydrology and Earth System Sciences, 15, 471–504, 2011.

Wagnon, P., Sicart, J. E., Berthier, E., and Chazarin, J. P.: Wintertime high-altitude surface energy balance of a Bolivian glacier, Illimani, 6340 m above sea level, J. Geophys. Res., 108, 4177, 2003.

Wilckzak, J. M., Oncley, S. P., and Stage, S. A.: Sonic Anemometer Tilt Correction Algorithms, Boundary-Layer Meteorol., 99, 127–150, 2001.

Wyngaard, J.: On surface layer turbulence, in: Haugen, D.A. (Ed.), Workshop on Micrometeorology. American Meteorological Society., 1973.

The Cryosphere Discuss., doi:10.5194/tc-2016-93, 2016
Manuscript under review for journal The Cryosphere
Published: 13 May 2016

Table 2. Characteristics of the two field campaigns in terms of WP frequencies, meteorological data, turbulence and turbulence fluxes. Fraction of runs recorded under each group of WPs, fraction of good-quality runs for the EC data in 2006, inside each group, and fraction of runs, inside each group during the 2009 campaign, for which a wind-speed maximum was observed with the profile mast. Mean meteorological variables recorded by the AWS-M, mean TKE in each weather group and turbulent fluxes measured with the EC and the BA methods with different roughness parameters.

	Strong Forcing		Weak forcing		Other forcing		2006-TKE	
	2006	2009	2006	2009	2006	2009	$\overline{e} < 1$ ms^{-2}	$\overline{e} > 2$ ms^{-2}
Time coverage	26%	46%	47%	33%	27%	21%	44%	38%
Fraction of good-quality runs (EC)	85%	-	75%	-	12%	-	49%	29%
Fraction of good-quality runs with a detected wind-speed maximum	-	31%	-	71%	-	72%	-	-
Fraction of runs in SF							28%	52%
Fraction of runs in WF							68%	11%
u_{AWS-M} [m s^{-1}]	5.2	5.5	2.5	2.6	3.0	2.6	2.6	4.4
T_{AWS-M} [°C]	7.2	9.1	7.6	5.3	2.9	4.4	6.7	5.7
q_{AWS-M} [10^{-3} kg kg^{-1}]	49	48	58	49	48	47	50	49
TKE [m^{-2} s^{-2}]	2.6	-	1.0	-	2.1	-	0.52	3.66
Fluxes [W m^{-2}]								
H_{EC}	45	-	24	-	21	-	18	47
LE_{EC}	-9	-	6	-	-9	-	4	-10
$H_b(z_{0,t,q})$	36	47	18	9	12	5	18	34
$LE_b(z_{0,t,q})$	3	3	6	-1	-3	-2	5	-2
$H_b(z_e)$	50	66	20	7	14	5	21	47
$LE_b(z_e)$	-6	4	7	-3	-4	-3	5	-5